Modeling and Control of a New Three-Input DC–DC Boost Converter for Hybrid PV/FC/Battery Power System

Farzam Nejabatkhah, *Member, IEEE*, Saeed Danyali, Seyed Hossein Hosseini, *Member, IEEE*, Mehran Sabahi, and Seyedabdolkhalegh Mozaffari Niapour, *Member, IEEE*

***Abstract*—A new three-input dc–dc boost converter is proposed in this paper. The proposed converter interfaces two unidirectional input power ports and a bidirectional port for a storage element in a unified structure. This converter is interesting for hybridizing alternative energy sources such as photovoltaic (PV) source, fuel cell (FC) source, and battery. Supplying the output load, charging or discharging the battery can be made by the PV and the FC power sources individually or simultaneously. The proposed structure utilizes only four power switches that are independently controlled with four different duty ratios. Utilizing these duty ratios, tracking the maximum power of the PV source, setting the FC power, controlling the battery power, and regulating the output voltage are provided. Depending on utilization state of the battery, three different power operation modes are defined for the converter. In order to design the converter control system, small-signal model is obtained in each operation mode. Due to interactions of converter control loops, decoupling network is used to design separate closed-loop controllers. The validity of the proposed converter and its control performance are verified by simulation and experimental results for different operation conditions.**

***Index Terms*—Decoupling method, photovoltaic/fuel cell (PV/FC)/battery hybrid power system, small-signal modeling, state-space averaging, three-input dc–dc boost converter.**

I. Introduction

NOWADAYS, photovoltaic (PV) energy appears quite attractive for electricity generation because of its noiseless, pollution-free, scale flexibility, and little maintenance. Because of the PV power generation dependence on sun irradiation level, ambient temperature, and unpredictable shadows, a PV-based power system should be supplemented by other alternative energy sources to ensure a reliable power supply. Fuel cells (FCs) are emerging as a promising supplementary power sources due to their merits of cleanness, high efficiency, and high reliability. Because of long startup period and slow dynamic response weak points of FCs [1], mismatch power between the load and the FC must be managed by an energy storage system. Batteries are usually taken as storage mechanisms for smoothing output power, improving startup transitions and dynamic characteristics, and enhancing the peak power capacity [2], [3]. Combining such energy sources introduces a PV/FC/battery hybrid power system. In comparison with single-sourced systems, the hybrid power systems have the potential to provide high quality, more reliable, and efficient power. In these systems with a storage element, the bidirectional power flow capability is a key feature at the storage port. Further, the input power sources should have the ability of supplying the load individually and simultaneously.

Many hybrid power systems with various power electronic converters have been proposed in the literature up to now. Traditional methods that integrate different power sources to form a hybrid power system can be classified into ac-coupled systems [4], [5] and ac-coupled systems [6]–[12]. However, the main shortcomings of these traditional integrating methods are complex system topology, high count of devices, high power losses, expensive cost, and large size. In recent years, several power conversion stages used in traditional hybrid systems are replaced by multi-input converters (MICs), which combine different power sources in a single power structure. These converters have received more attention in the literature because of providing simple circuit topology, centralized control, bidirectional power flow for the storage element, high reliability, and low manufacturing cost and size. In general, the systematic approach of generating MICs is introduced in [13], in which the concept of the pulsating voltage source cells and the pulsating current source cells is proposed for deriving MICs. One of the samples of these MICs is utilized in [14] to hybridize PV and wind power sources in a unified structure. Besides, a systematic method to synthesize MICs is proposed in [15]. This paper deals with two types of MICs: in the first type, only one power source is allowed to transfer energy to the load at a time, and in the second type, all the input sources can deliver power to the load either individually or simultaneously. As another basic research in MICs, in [16] assumptions, restrictions, and conditions used in analyzing MICs are described, and then it lists some basic rules that allow determining feasible and unfeasible input cells that realize MICs from their single-input versions. Two multiple-input converters based on flux additivity in a multiwinding transformer are reported in [17] and [18]. Because there was no possibility of bidirectional operating of the converter in [17], and complexity of driving circuits and output power limitation in [18], they are not suitable for hybrid

Manuscript received April 10, 2011; revised June 29, 2011 and August 23, 2011; accepted October 4, 2011. Date of current version February 27, 2012. Recommended for publication by Associate Editor S. Choi.

The authors are with the Faculty of Electrical and Computer Engineering, University of Tabriz, 51666-16471 Tabriz, Iran (e-mail: farzamnejabatkhah@gmail.com; danyali.tabrizu@gmail.com; hosseini@tabrizu.ac.ir; sabahi@tabrizu.ac.ir; mozafari.tabrizu@gmail.com).

Color versions of one or more of the figures in this paper are available online at http://ieeexplore.ieee.org.

Digital Object Identifier 10.1109/TPEL.2011.2172465

systems. In [19], a three-port bidirectional converter with three active full bridges, two series-resonant tanks, and a three-winding high-frequency transformer are proposed. In comparison with three-port circuits with only inductors and diode bridge at the load side, it gives higher boost gain and reduced switching losses due to soft-switching operation.

H. Tao *et al*. [20] present a family of multiport converters based on combination of dc link and magnetic coupling by utilizing half-bridge boost converters. The system features minimum number of conversion steps, low cost, and compact packaging. In [21], the input–output feedback control linearization for a dc–ac bidirectional MIC composing a high-frequency isolating link transformer, two half-bridge boost converters at the input ports and a bidirectional cycloconverter at the output port is proposed. In [22]–[24], three MICs are proposed based on structure of the dc–dc boost converter. The dc–dc boost converter in [22] is useful for combining several energy sources whose power capacity or voltage levels are different. The multi-input dc–dc converter proposed in [23] has the capability of operating in different converter topologies (buck, boost, and buck–boost) in addition to its bidirectional operation and positive output voltage without any additional transformer. A three-input dc–dc boost converter proposed by authors in [24] can combine a PV, an FC, and a battery in a simple unified structure. A comprehensive power management algorithm is realized in order to achieve maximum power point tracking (MPPT) of the PV source and set the FC in its optimal power operation range. A three-port isolated full-bridge topology is proposed in [3] for hybrid FC/battery system, which its aim is feeding a small autonomous load. This topology gains the advantage of bidirectional power flow due to the active full-bridges in each port. Based on the model of the transformer reported in [3], the three transformer-coupled half-bridge converters proposed in [25] are analyzed. Thereby, phase-shift control method is used to manage the power flow among the three ports in addition to soft switching for all switches over a wide input range. Wai *et al*. presents two kinds of MICs in [2] and [26]. In [26], a high step-up ratio bidirectional MIC with high-efficiency is proposed. The converter operates in stand-alone state, united power supply state, and charge and discharge states. A two-input power converter for a hybrid FC/battery power system is proposed in [2] with zero-voltage switching characteristic. Although the circuit efficiency is greatly developed, the converter does not provide bidirectional functionality and is not able to boost the input voltage to a higher level. Moreover, the summation of duty ratios should be greater than 1 and the two input voltages should be in the same level in the dual-power-supply operation state. Qian *et al*. presents a hybrid power system consist of a PV and a battery in [27] for satellite applications, and a four-port hybrid power system supplied by a PV, a wind, and a battery in [28]. In [27], a power control strategy is designed to manage the charge balance of the battery in order to regulate the output voltage. In these systems, the PV and the wind sources are exploited in MPPT conditions. Moreover, control strategies of the both systems are designed based on small-signal modeling of the converters. Proper decoupling method is productively introduced to separately design compensators for cross-coupled control loops.

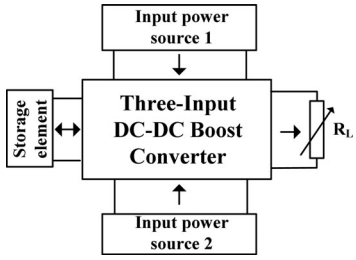

Fig. 1. Proposed system overview.

In this paper, a new three-input dc–dc boost converter is proposed for hybrid power system applications. As shown in Fig. 1, the proposed converter interfaces two unidirectional ports for input power sources, a bidirectional port for a storage element, and a port for output load in a unified structure. The converter is current-source type at the both input power ports and is able to step up the input voltages. The proposed structure utilizes only four power switches that are independently controlled with four different duty ratios. Utilizing these duty ratios facilitates controlling the power flow among the input sources and the load. Powers from the input power sources can be delivered to the load individually or simultaneously. Moreover, the converter topology enables the storage element to be charged or discharged through both input power sources. Depending on utilization state of the storage element; three different power operation modes of the converter are defined. Besides, in order to design the control system, converter small-signal model is obtained in each operation mode. Due to multivariable nature of the control system, decoupling network is utilized in order to separately design closed-loop controllers. In comparison with the conventional method of hybridizing three input sources with three-boost cells [30], the proposed converter can economize in the number of inductors, makes use of low-voltage batteries or super capacitors, works in high-stable-margin operating points and gain access to high-voltage boost factor. As another improvement in our proposed system in comparison with converter represented in [24], the battery can be charged and discharged through the both power sources individually and simultaneously. Also, four duty ratios of the converter are controlled independently, so the restriction of the duty ratios summation is eliminated which results in high level of the output voltage. All in all, the proposed converter is a good alternative for the multiple-source hybrid power systems and has the merits of including bidirectional power flow at the storage port, simple structure, low-power components, centralized control, no need to transformer, low weight, high-stability working point, independent operation of input power sources, and high level of boosting.

As an interesting application of the proposed converter, the input ports are mainly considered to interface a PV source and an FC source, and a battery as the storage element. In this application, achieving the maximum power of the PV source, setting power of the FC, charging or discharging the battery, and also regulating the output voltage are realized by utilizing the converter duty ratios.

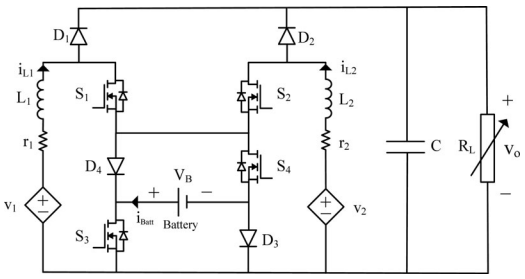

Fig. 2. Circuit topology of the proposed system.

This paper is organized as follows. The converter structure and operation modes are explained in Section II. The dynamic modeling of the proposed converter is given in Section III. Section IV describes the control system of the proposed converter. The system power operation mode determination is discussed in Section V. Section VI represents the simulation and experimental verifications and Section VII concludes this paper.

II. Converter Structure and Operation Modes

The structure of the proposed three-input dc–dc boost converter is represented in Fig. 2. As seen from the figure, the converter interfaces two input power sources v_1 and v_2, and a battery as the storage element. The proposed converter is suitable alternative for hybrid power systems of PV, FC, and wind sources. Therefore, v_1 and v_2 are shown as two dependent power sources that their output characteristics are determined by the type of input power sources. For example, for a PV source at the first port, v_1 is identified as a function of its current i_{L1}, light intensity, and ambient temperature. In the converter structure, two inductors L_1 and L_2 make the input power ports as two current-type sources, which result in drawing smooth dc currents from the input power sources. The R_L is the load resistance, which can represent the equivalent power feeding an inverter. Four power switches S_1, S_2, S_3, and S_4 in the converter structure are the main controllable elements that control the power flow of the hybrid power system. The circuit topology enables the switches to be independently controlled through four independent duty ratios d_1, d_2, d_3, and d_4, respectively. As like as the conventional boost converters, diodes D_1 and D_2 conduct in complementary manner with switches S_1 and S_2. The converter structure shows that when switches S_3 and S_4 are turned ON, their corresponding diodes D_3 and D_4 are reversely biased by the battery voltage and then blocked. On the other hand, turn-OFF state of these switches makes diodes D_3 and D_4 able to conduct input currents i_{L1} and i_{L2}. In hybrid power system applications, the input power sources should be exploited in continuous current mode (CCM). For example, in the PV or FC systems, an important goal is to reach an acceptable current ripple in order to set their output power on desired value. Therefore, the current ripple of the input sources should be minimized to make an exact power balance among the input powers and the load. Therefore, in this paper, steady state and dynamic behavior of the converter have been investigated in CCM.

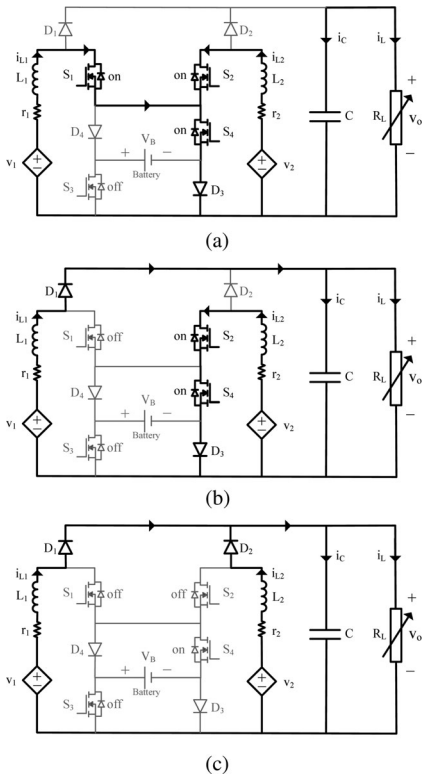

Fig. 3. First operation mode. (a) Switching state 1: $0 < t < d_1T$. (b) Switching state 2: $d_1T < t < d_2T$. (c) Switching state 3: $d_2T < t < T$.

In general, depending on utilization state of the battery, three power operation modes are defined to the proposed converter. These modes of operation are investigated with the assumptions of utilizing the same sawtooth carrier waveform for all the switches, and d_3,$d_4 < \min(d_1,d_2)$ in battery charge or discharge mode. Although exceeding duty ratios d_3 and d_4 from d_1 or d_2 does not cause converter malfunction, it results in setting the battery power on the possible maximum values. In order to simplify the investigations, it is assumed that duty ratio d_1 is less than duty ratio d_2. Further, with the assumption of ideal switches, the steady-state equations are obtained in each operation mode.

A. First Power Operation Mode (Supplying the Load With Sources v_1 and v_2 Without Battery Existence)

In this operation mode, two input power sources v_1 and v_2 are responsible for supplying the load, and battery charging/discharging is not done. This operation mode is considered as the basic operation mode of the converter. As clearly seen from the converter structure, there are two options to conduct input power sources currents i_{L1} and i_{L2} without passing through the battery; path 1: S_4–D_3, path 2: S_3–D_4. In this operation mode, the first path is chosen; therefore, switch S_3 is turned OFF while switch S_4 is turned ON entirely in the switching period ($d_4 = 1$ and $d_3 = 0$). Thus, three different switching states of the converter are achieved in one switching period. These switching states are depicted in Fig. 3(a)–(c). Also, the steady-state waveforms of the gate signals of the four switches

and the variations of inductors currents i_{L1} and i_{L2} are shown in Fig. 6(a).

Switching state 1 ($0 < t < d_1\,T$): At $t = 0$, switches S_1 and S_2 are turned ON and inductors L_1 and L_2 are charged with voltages across v_1 and v_2, respectively [see Fig. 3(a)].

Switching state 2 ($d_1\,T < t < d_2\,T$): At $t = d_1T$, switch S_1 is turned OFF, while switch S_2 is still ON (according to the assumption $d_1 < d_2$). Therefore, inductor L_1 is discharged with voltage across $v_1 - v_o$ into the output load and the capacitor through diode D_1, while inductor L_2 is still charged by voltage across v_2 [see Fig. 3(b)].

Switching state 3 ($d_2T < t < T$): At $t = d_2T$, switch S_2 is also turned OFF and inductor L_2 is discharged with voltage across $v_2 - v_o$, as like as inductor L_1 [see Fig. 3(c)].

By applying voltage–second and current–second balance theory [29] to the converter, following equations are obtained:

$$L_1 : d_1T(v_1 - r_1 i_{L_1}) + (1 - d_1)T(v_1 - r_1 i_{L_1} - v_o) = 0 \rightarrow v_o = \frac{v_1 - r_1 i_{L_1}}{1 - d_1} \quad (1)$$

$$L_2 : d_2T(v_2 - r_2 i_{L_2}) + (1 - d_2)T(v_2 - r_2 i_{L_2} - v_o) = 0 \rightarrow v_o = \frac{v_2 - r_2 i_{L_2}}{1 - d_2} \quad (2)$$

$$C : (1 - d_1)T i_{L_1} + (1 - d_2)T i_{L_2} = T\frac{v_o}{R_L} \quad (3)$$

$$i_{\text{batt}} = 0 \rightarrow P_{\text{batt}} = 0. \quad (4)$$

In this operation mode, the control strategy is based on regulating one of the input sources on its reference power with its corresponding duty ratio, while the other power source is utilized to regulate the output voltage by means of its duty ratio.

B. Second Power Operation Mode (Supplying the Load With Sources v_1 and v_2 and the Battery)

In this operation mode, two input power sources v_1 and v_2 along with the battery are responsible for supplying the load. Therefore, discharging state of the battery should be provided in this operation mode. Referring to the converter topology, when switches S_3 and S_4 are turned ON simultaneously, currents i_{L1} and i_{L2} are conducted through the path of switch S_4, the battery, and switch S_3 which results in battery discharging. However, discharging operations of the battery can only last until switches S_1 and/or S_2 are conducting. As a result, the maximum discharge power of the battery depends on duty ratios of d_1 and d_2 as well as currents i_{L1} and i_{L2}:

$$P_{\text{bat.dis}}^{\max} = v_B\left[d_1 i_{L_1} + d_2 i_{L_2}\right], \quad S_3 = \text{ON}, S_4 = \text{ON}. \quad (5)$$

Therefore, in order to acquire a desired maximum discharging power of the battery, the input power sources should be designed in proper current and voltage values. On the other hand, regulating the discharging power of the battery below $P_{\text{bat.dis}}^{\max}$ can be made by changing the state of only one of switches S_3 and S_4 before switches S_1 and S_2 are turned OFF (according to the assumption d_3,$d_4 < \min(d_1,d_2)$). In this paper, duty ratio d_4 is controlled to regulate the discharging power of the battery regarding the facts that when S_4 is turned ON, it results in passing the currents of input power sources through the battery; hence, the battery discharge mode is started, and its turn-OFF state starts conducting through diode D_4 and stops discharging the battery. As depicted in Fig. 4(a)–(d), there are four different switching states for the converter in one switching period. The steady-state waveforms of the gate signals of the four switches and the variations of input currents i_{L1} and i_{L2} are shown in Fig. 6(b).

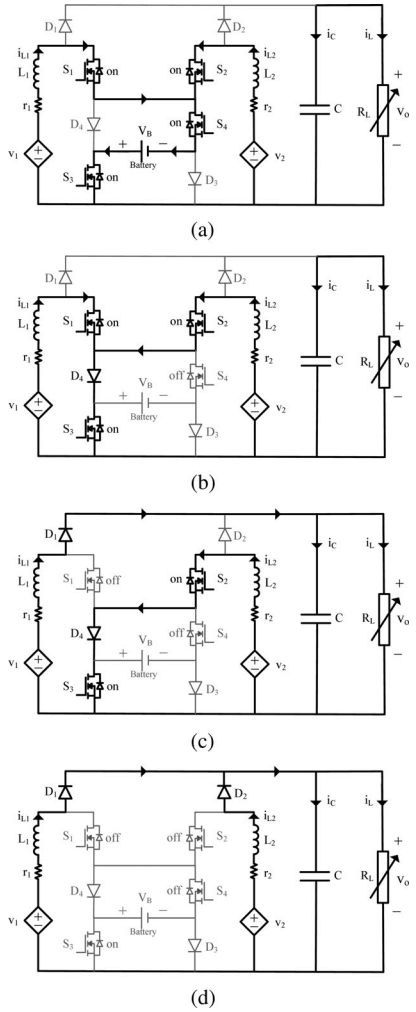

Fig. 4. Second operation mode. (a) Switching state 1: $0 < t < d_4T$. (b) Switching state 2: $d_4T < t < d_1T$. (c) Switching state 3: $d_1T < t < d_2T$. (d) Switching state 4: $d_2T < t < T$.

Switching state 1 ($0 < t < d_4T$): At $t = 0$, switches S_1, S_2, and S_4 are turned ON, so inductors L_1 and L_2 are charged with voltages across $v_1 + v_B$ and $v_2 + v_B$, respectively [see Fig. 4(a)].

Switching state 2 ($d_4T < t < d_1T$): At $t = d_4T$, switch S_4 is turned OFF, while switches S_1 and S_2 are still ON. Therefore, inductors L_1 and L_2 are charged with voltages across v_1 and v_2, respectively [see Fig. 4(b)].

Switching state 3 ($d_1T < t < d_2T$): At $t = d_1T$, switch S_1 is turned OFF, so inductor L_1 is discharged with voltage across v_1

$- v_o$, while inductor L_2 is still charged with voltages across v_2 [see Fig. 4(c)].

Switching state 4 ($d_2T < t < T$): At $t = d_2T$, switch S_2 is also turned OFF and inductors L_1 and L_2 are discharged with voltage across $v_1 - v_o$ and $v_2 - v_o$, respectively [see Fig. 4(d)].

By applying voltage–second and current–second balance theory to the converter, following equations are obtained:

$$L_1 : d_4T(v_1 - r_1 i_{L_1} + v_B) + (d_1 - d_4)T(v_1 - r_1 i_{L_1}) + (1 - d_1)T(v_1 - r_1 i_{L_1} - v_o) = 0$$
$$\rightarrow v_o = \frac{v_1 - r_1 i_{L_1} + d_4 v_B}{1 - d_1} \tag{6}$$

$$L_2 : d_4T(v_2 - r_2 i_{L_2} + v_B) + (d_2 - d_4)T(v_2 - r_2 i_{L_2}) + (1 - d_2)T(v_2 - r_2 i_{L_2} - v_o) = 0$$
$$\rightarrow v_o = \frac{v_2 - r_2 i_{L_2} + d_4 v_B}{1 - d_2} \tag{7}$$

$$C : (1 - d_1)T i_{L_1} + (1 - d_2)T i_{L_2} = T\frac{v_o}{R_L} \tag{8}$$

$$\text{Battery} \begin{cases} i_{\text{Batt}} = d_4(i_{L_1} + i_{L_2}) \\ P_{\text{Batt}} = v_B[d_4(i_{L_1} + i_{L_2})]. \end{cases} \tag{9}$$

In this operation mode, the control strategy is based on regulating both of the input power sources on their reference powers by means of their corresponding duty ratios d_1 and d_2, while the battery discharge power is utilized to regulate the output voltage by duty ratio d_4.

C. Third Power Operation Mode (Supplying the Load With Sources v_1 and v_2, and Battery Charging Performance)

In this operation mode, two input power sources v_1 and v_2 are responsible for supplying the load while the battery charging performance is accomplished. Therefore, the charging state of the battery should be provided in this operation mode. Referring to the converter topology, when switches S_3 and S_4 are turned OFF, by turning ON switches S_1 and S_2, currents i_{L1} and i_{L2} are conducted through the path of diode D_4, the battery, and diode D_3; therefore, the condition of battery charging is provided. However, the charging operation of the battery can only last until switches S_1 and/or S_2 are conducting. As a result, the maximum charge power of the battery depends on duty ratios d_1 and d_2 as well as currents i_{L1} and i_{L2}:

$$P_{\text{bat.ch}}^{\max} = -v_B\left[d_1 i_{L_1} + d_2 i_{L_2}\right], \quad S_3 = \text{OFF}, S_4 = \text{OFF}. \tag{10}$$

Therefore, in order to acquire a desired maximum charge power of the battery, the input power sources should be designed in proper current and voltage values. On the other hand, regulating the charging power of the battery below the $P_{\text{bat.ch}}^{\max}$ can be made by changing the state of only one of switches S_3 and S_4 before switches S_1 and S_2 are turned OFF (according to the assumption d_3,$d_4 < \min(d_1,d_2)$). In this paper, in order to regulate the charging power of the battery, switch S_3 is controlled by regarding the fact that when switch S_3 is turned ON, the charging power of the battery is not accomplished while its turn-OFF state make the battery to be charged with currents i_{L1} and i_{L2} through the path of D_3. Four different switching states occurred in one switching period are illustrated in Fig. 5(a)–(d). Also, the steady-state waveforms of the gate signals of the four switches and the variations of input currents i_{L1} and i_{L2} are shown in the Fig. 6(c).

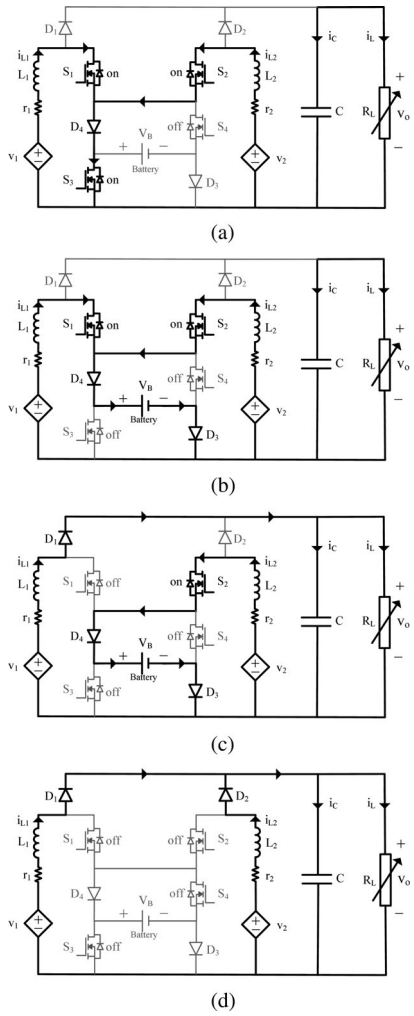

Fig. 5. Third operation mode. (a) Switching state 1: $0 < t < d_3T$. (b) Switching state 2: $d_3T < t < d_1T$. (c) Switching state 3: $d_1T < t < d_2T$. (d) Switching state 4: $d_2T < t < T$.

Switching state 1 ($0 < t < d_3\ T$): At $t = 0$, switches S_1, S_2, and S_3 are turned ON, so inductors L_1 and L_2 are charged with voltages across v_1 and v_2, respectively [see Fig. 5(a)].

Switching state 2 ($d_3\ T < t < d_1\ T$): At $t = d_3\ T$, switch S_3 is turned OFF while switches S_1 and S_2 are still ON (according to the assumption). Therefore, inductors L_1 and L_2 are charged with voltages across $v_1 - v_B$ and $v_2 - v_B$, respectively [see Fig. 5(b)].

Switching state 3 ($d_1\ T < t < d_2\ T$): At $t = d_1\ T$, switch S_1 is turned OFF, so inductor L_1 is discharged with voltage across $v_1 - v_o$, while inductor L_2 is still charged with voltage across $v_2 - v_B$ [see Fig. 5(c)].

Switching state 4 ($d_2\ T < t < T$): At $t = d_2\ T$, switch S_2 is also turned OFF and inductor L_2 as like as L_1 is discharged with voltage across $v_2 - v_o$ [see Fig. 5(d)].

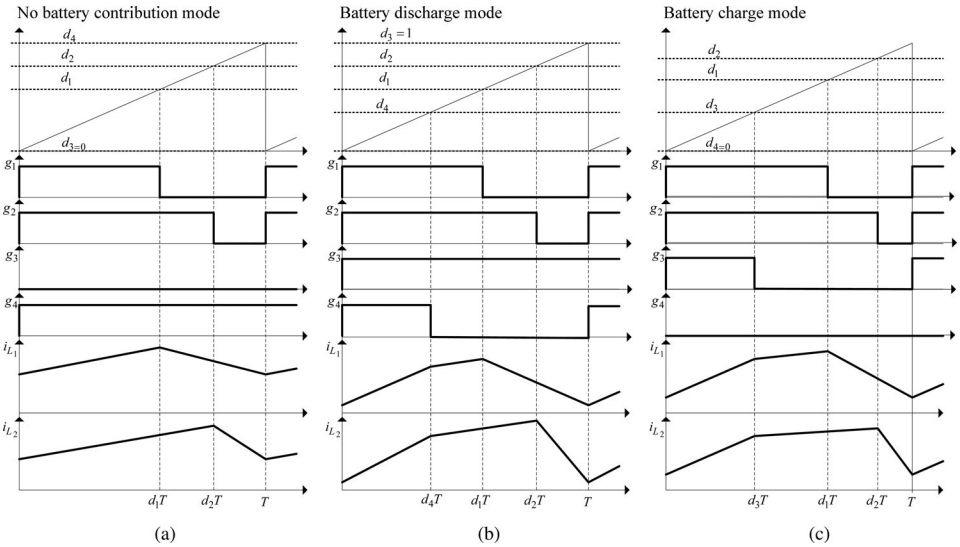

Fig. 6. Steady-state waveform of proposed converter in (a) first operation mode, (b) second operation mode, and (c) third operation mode.

By applying voltage–second and current–second balance theory to the converter, following equations are obtained:

$$L_1 : d_3T(v_1 - r_1 i_{L_1}) + (d_1 - d_3)T(v_1 - r_1 i_{L_1} - v_B) + (1 - d_1)T(v_1 - r_1 i_{L_1} - v_o) = 0$$
$$\rightarrow v_o = \frac{v_1 - r_1 i_{L_1} - (d_1 - d_3)v_B}{1 - d_1} \tag{11}$$

$$L_2 : d_2T(v_2 - r_2 i_{L_2}) + (d_2 - d_3)T(v_2 - r_2 i_{L_2} - v_B) + (1 - d_2)T(v_2 - r_2 i_{L_2} - v_o) = 0$$
$$\rightarrow v_o = \frac{v_2 - r_2 i_{L_2} - (d_2 - d_3)v_B}{1 - d_2} \tag{12}$$

$$C : (1 - d_1)Ti_{L_1} + (1 - d_2)Ti_{L_2} = T\frac{v_o}{R_L} \tag{13}$$

$$\text{Battery} \begin{cases} i_{\text{Batt}} = -(d_1 - d_3)i_{L_1} - (d_2 - d_3)i_{L_2} \\ P_{\text{Batt}} = -v_B[(-d_3)(i_{L_1} + i_{L_2}) + d_1 i_{L_1} + d_2 i_{L_2}]. \end{cases} \tag{14}$$

In this operation mode, if the total generated power of the input sources becomes more than the load power, the battery charging performance will be possible if duty ratio d_3 is utilized to regulate the output voltage. With this control strategy, duty ratios d_1 and d_2 are utilized to regulate powers of the input sources, while duty ratio d_3 is utilized to regulate the output voltage through charging the battery by the extra-generated power.

In all three operation modes, when one of the input power sources is not present to produce power, its corresponding duty ratio is set at zero, which results single power source operation for the converter.

III. Dynamic Modeling of the Proposed Converter

The proposed converter can operate in three different power operation modes. Controlling the converter in each operation mode requires different control variables to regulate the powers of input sources and the output voltage. First power operation mode utilizes two active duty ratios, while in the second and third operation modes three different duty ratios are chosen. Therefore, a multi-input multioutput (MIMO) control system is introduced to the converter. Due to several interaction control loops in the MIMO systems, designing closed-loop controllers for such systems is difficult. However, decoupling network is a proper control method that allows designing separate closed-loop controllers for MIMO systems. In order to design closed-loop controllers for the proposed MIC, the small-signal model of the converter should be obtained first. This model can demonstrate the converter transient behavior and its stability, and facilitates proper design of the converter controllers [30]. The state variables of the converter are i_{L1}, i_{L2}, and v_o. State-space averaged model of the converter in each operation modes is investigated as follows.

First operation mode: In this mode, three state variables are controlled by two control variables d_1 and d_2. Therefore, the state-space averaged model is shown in

$$L_1\frac{di_{L_1}}{dt} = d_1 v_1 + (1 - d_1)(v_1 - v_o) - r_1 i_{L_1}$$
$$L_2\frac{di_{L_2}}{dt} = d_2 v_2 + (1 - d_2)(v_2 - v_o) - r_2 i_{L_2}$$
$$C\frac{dv_o}{dt} = (1 - d_1)i_{L_1} + (1 - d_2)i_{L_2} - \frac{v_o}{R_L}. \tag{15}$$

Second operation mode: In this mode, three control variables d_1, d_2, and d_4 are controlled to regulate all three state variables. Therefore, the state-space averaged model is shown in

$$L_1\frac{di_{L_1}}{dt} = (d_1 - d_4)v_1 + d_4(v_1 + v_B) + (1 - d_1)(v_1 - v_o) - r_1 i_{L_1}$$
$$L_2\frac{di_{L_2}}{dt} = (d_2 - d_4)v_2 + d_4(v_2 + v_B)$$

$$+(1-d_2)(v_2-v_o)-r_2 i_{L_2}$$
$$C\frac{dv_o}{dt}=(1-d_1)i_{L_1}+(1-d_2)i_{L_2}-\frac{v_o}{R_L}. \quad (16)$$

Third operation mode: Three control variables d_1, d_2, and d_3 are controlled to regulate all three state variables. Therefore, the state-space averaged model is shown in

$$L_1\frac{di_{L_1}}{dt}=d_3v_1+(d_1-d_3)(v_1-v_B)+(1-d_1)(v_1-v_o)-r_1i_{L_1}$$
$$L_2\frac{di_{L_2}}{dt}=d_3v_2+(d_2-d_3)(v_2-v_B)+(1-d_2)(v_2-v_o)-r_2i_{L_2}$$
$$C\frac{dv_o}{dt}=(1-d_1)i_{L_1}+(1-d_2)i_{L_2}-\frac{v_o}{R_L}. \quad (17)$$

Based on small-signal modeling method [27], [31], the state variables, duty ratios, and input voltages contain two components: dc values $(\bar{X},\bar{D},\bar{V})$ and perturbations $(\tilde{x},\tilde{d},\tilde{v})$:

$$x=\bar{X}+\tilde{x};\quad d=\bar{D}+\tilde{d};\quad v=\bar{V}+\tilde{v}. \quad (18)$$

It is assumed that the perturbations are small and do not vary significantly during one switching period $(\tilde{x}\ll\bar{X},\tilde{d}\ll\bar{D},\tilde{v}\ll\bar{X})$. Substituting (18) into (15)–(17) and neglecting the second-order terms, small-signal models are resulted. The small-signal models are represented in matrix form as follows:

$$\dot{\tilde{x}}=A\tilde{x}+B\tilde{u}$$
$$\tilde{y}=C\tilde{x}+D\tilde{u} \quad (19)$$

where $\tilde{x}$, $\tilde{u}$, and $\tilde{y}$ are state variable vector, control variables vector, and system output vector. Therefore, the matrix forms of the small-signal models for the first, second, and third operation modes are obtained as follows.

First mode:

$$A=\begin{bmatrix}\frac{-r_1}{L_1}&0&\frac{\bar{D}_1-1}{L_1}\\0&\frac{-r_2}{L_2}&\frac{\bar{D}_2-1}{L_2}\\\frac{1-\bar{D}_1}{C}&\frac{1-\bar{D}_2}{C}&\frac{-1}{R_LC}\end{bmatrix};B=\begin{bmatrix}\frac{\bar{V}_o}{L_1}&0\\0&\frac{\bar{V}_o}{L_2}\\\frac{-\bar{I}_{L_1}}{C}&\frac{-\bar{I}_{L_2}}{C}\end{bmatrix}$$
$$\tilde{x}=\begin{bmatrix}\tilde{i}_{L_1}\\\tilde{i}_{L_2}\\\tilde{v}_o\end{bmatrix};\quad \tilde{u}=\begin{bmatrix}\tilde{d}_1\\\tilde{d}_2\end{bmatrix};\quad C=\begin{bmatrix}1&0&0\\0&0&0\\0&0&1\end{bmatrix};\quad D=0. \quad (20)$$

Second mode:

$$A=\begin{bmatrix}\frac{-r_1}{L_1}&0&\frac{\bar{D}_1-1}{L_1}\\0&\frac{-r_2}{L_2}&\frac{\bar{D}_2-1}{L_2}\\\frac{1-\bar{D}_1}{C}&\frac{1-\bar{D}_2}{C}&\frac{-1}{R_LC}\end{bmatrix}$$
$$B=\begin{bmatrix}\frac{\bar{V}_o}{L_1}&0&\frac{\bar{V}_B}{L_1}\\0&\frac{\bar{V}_o}{L_2}&\frac{\bar{V}_B}{L_2}\\\frac{-\bar{I}_{L_1}}{C}&\frac{-\bar{I}_{L_2}}{C}&0\end{bmatrix};\quad \tilde{x}=\begin{bmatrix}\tilde{i}_{L_1}\\\tilde{i}_{L_2}\\\tilde{v}_o\end{bmatrix}$$
$$\tilde{u}=\begin{bmatrix}\tilde{d}_1\\\tilde{d}_2\\\tilde{d}_4\end{bmatrix};\quad C=\begin{bmatrix}1&0&0\\0&1&0\\0&0&1\end{bmatrix};\quad D=0. \quad (21)$$

Third mode:

$$A=\begin{bmatrix}\frac{-r_1}{L_1}&0&\frac{\bar{D}_1-1}{L_1}\\0&\frac{-r_2}{L_2}&\frac{\bar{D}_2-1}{L_2}\\\frac{1-\bar{D}_1}{C}&\frac{1-\bar{D}_2}{C}&\frac{-1}{R_LC}\end{bmatrix}$$
$$B=\begin{bmatrix}\frac{\bar{V}_o-\bar{V}_B}{L_1}&0&\frac{\bar{V}_B}{L_1}\\0&\frac{\bar{V}_o-\bar{V}_B}{L_2}&\frac{\bar{V}_B}{L_2}\\\frac{-\bar{I}_{L_1}}{C}&\frac{-\bar{I}_{L_2}}{C}&0\end{bmatrix};\quad \tilde{x}=\begin{bmatrix}\tilde{i}_{L_1}\\\tilde{i}_{L_2}\\\tilde{v}_o\end{bmatrix}$$
$$\tilde{u}=\begin{bmatrix}\tilde{d}_1\\\tilde{d}_2\\\tilde{d}_3\end{bmatrix};\quad C=\begin{bmatrix}1&0&0\\0&1&0\\0&0&1\end{bmatrix};\quad D=0. \quad (22)$$

IV. Control System Description

As represented in the system small-signal models, state variables are controlled by two or three control variables. The transfer function matrix of the converter is obtained from the small-signal model as follows:

$$G=C(sI-A)^{-1}B+D. \quad (23)$$

The rank of transfer function matrix denotes the number of control variables. In this paper, according to the number of control variables and based on (23), two different $G_{3\times3}$-type transfer function matrixes are obtained to the second and third operation modes, while a $G_{2\times2}$-type is considered for the first operation mode as follows:

$$\underbrace{\begin{bmatrix}y_1\\y_2\end{bmatrix}}_{y}=\underbrace{\begin{bmatrix}g_{11}&g_{12}\\g_{21}&g_{22}\end{bmatrix}}_{G_{2\times2}}\underbrace{\begin{bmatrix}u_1\\u_2\end{bmatrix}}_{u} \quad (24)$$

$$\underbrace{\begin{bmatrix}y_1\\y_2\\y_3\end{bmatrix}}_{y}=\underbrace{\begin{bmatrix}g_{11}&g_{12}&g_{13}\\g_{21}&g_{22}&g_{23}\\g_{31}&g_{32}&g_{33}\end{bmatrix}}_{G_{3\times3}}\underbrace{\begin{bmatrix}u_1\\u_2\\u_3\end{bmatrix}}_{u} \quad (25)$$

where y and u are the system output and input vectors, and component g_{ij} represents the transfer function between y_i and u_j. In order to separately design closed-loop compensators for the coupled control loops, decoupling method is introduced [32]. Such a decoupling network is considered in system controller design procedure although not included in the compensators. Fig. 7 shows the converter model in the three

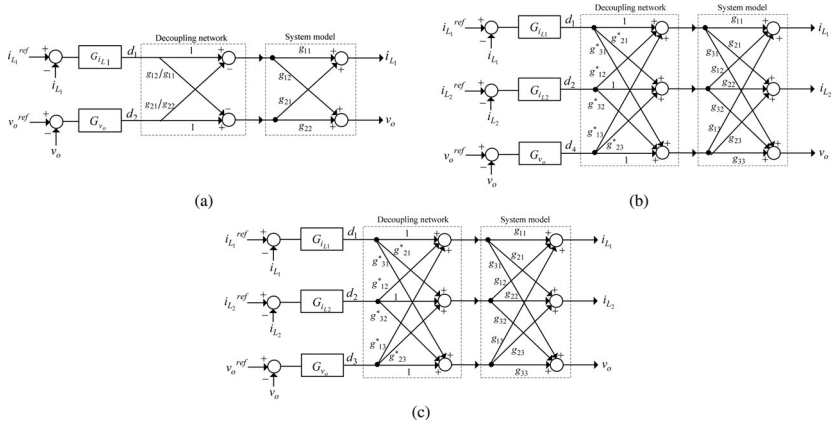

Fig. 7. Converter model accompanied with decoupling network and closed-loop compensators in (a) the first operation mode, (b) the second operation mode, and (c) the third operation mode.

operation modes accompanied with decoupling networks and closed-loop compensators. In general description of decoupling network G^* derivation [27], [28], [32], the state vector x can be written as $x = Gu^*$, where u^* is the modified input vector made up of duty ratios $u^* = G^*u$. Therefore, $x = GG^*u$. According to modern control theory, our goal is to make GG^* a diagonal matrix to allow one control input to determine one output, independently [27]. Based on $G^* = G^{-1}xu^{-1}$, decoupling matrixes $G^*_{2\times2}$ and $G^*_{3\times3}$ are achieved

$$G^*_{2\times2} = \begin{bmatrix} 1 & -\dfrac{g_{12}}{g_{11}} \\ -\dfrac{g_{21}}{g_{22}} & 1 \end{bmatrix} \tag{26}$$

$$G^*_{3\times3} = \begin{bmatrix} 1 & \dfrac{g_{13}\cdot g_{32} - g_{12}\cdot g_{33}}{g_{11}\cdot g_{33} - g_{13}\cdot g_{31}} & \dfrac{g_{12}\cdot g_{23} - g_{13}\cdot g_{22}}{g_{11}\cdot g_{22} - g_{12}\cdot g_{21}} \\ \dfrac{g_{23}\cdot g_{31} - g_{21}\cdot g_{33}}{g_{22}\cdot g_{33} - g_{23}\cdot g_{32}} & 1 & \dfrac{g_{13}\cdot g_{21} - g_{11}\cdot g_{23}}{g_{11}\cdot g_{22} - g_{12}\cdot g_{21}} \\ \dfrac{g_{21}\cdot g_{32} - g_{22}\cdot g_{31}}{g_{22}\cdot g_{33} - g_{23}\cdot g_{32}} & \dfrac{g_{12}\cdot g_{31} - g_{11}\cdot g_{32}}{g_{11}\cdot g_{33} - g_{13}\cdot g_{31}} & 1 \end{bmatrix}. \tag{27}$$

Utilizing decoupling network $G^*_{2\times2}$ makes cross-coupled two-loop control system $G_{2\times2}$ to be decoupled into two independent single-loop control systems as follows:

$$\frac{y_1}{u_1} = g_{11} - g_{12}\frac{g_{21}}{g_{22}}$$
$$\frac{y_2}{u_2} = -g_{12}\frac{g_{21}}{g_{11}} + g_{22}. \tag{28}$$

Similarly, three independent single-loop control systems are achieved using decoupling network $G^*_{3\times3}$ for the cross-coupled three-loop control system of $G_{3\times3}$ as follows:

$$\frac{y_1}{u_1} = g_{11} + g_{12}\frac{g_{13}\cdot g_{32} - g_{12}\cdot g_{33}}{g_{11}\cdot g_{33} - g_{13}\cdot g_{31}} + g_{13}\frac{g_{12}\cdot g_{23} - g_{13}\cdot g_{22}}{g_{11}\cdot g_{22} - g_{12}\cdot g_{21}}$$
$$\frac{y_2}{u_2} = g_{21}\frac{g_{23}\cdot g_{31} - g_{21}\cdot g_{33}}{g_{22}\cdot g_{33} - g_{23}\cdot g_{32}} + g_{22} + g_{23}\frac{g_{13}\cdot g_{21} - g_{11}\cdot g_{23}}{g_{11}\cdot g_{22} - g_{12}\cdot g_{21}}$$
$$\frac{y_3}{u_3} = g_{31}\frac{g_{21}\cdot g_{32} - g_{22}\cdot g_{31}}{g_{22}\cdot g_{33} - g_{23}\cdot g_{32}} + g_{32}\frac{g_{12}\cdot g_{31} - g_{11}\cdot g_{32}}{g_{11}\cdot g_{33} - g_{13}\cdot g_{31}} + g_{33}. \tag{29}$$

TABLE I
CONTROL SYSTEM COMPENSATORS

Operation mode	First	Second	Third
G_{vo}	$K = 2023.1\times10^{-5}$ $T = 3331.4\times10^{-5}$ $aT = 15.70\times10^{-6}$	$K = 1583.5\times10^{-4}$ $T = 1489.3\times10^{-5}$ $aT = 5.62\times10^{-6}$	$K = 4043.6\times10^{-4}$ $T = 454.3\times10^{-5}$ $aT = 22.3\times10^{-6}$
$G_{i_{L1}}$	$K = 34948.6\times10^{-4}$ $T = 205.6\times10^{-5}$ $aT = 76.97\times10^{-6}$	$K = 9855\times10^{-4}$ $T = 749.1\times10^{-5}$ $aT = 19.16\times10^{-6}$	$K = 1617.1\times10^{-4}$ $T = 1375.8\times10^{-5}$ $aT = 5.11\times10^{-6}$
$G_{i_{L2}}$	×	$K = 3257.2\times10^{-4}$ $T = 526.0\times10^{-5}$ $aT = 20.05\times10^{-6}$	$K = 4884.1\times10^{-4}$ $T = 1294.4\times10^{-5}$ $aT = 5.43\times10^{-6}$

Utilizing (28) and (29), the transfer functions of the decoupled system are obtained for each operation mode. Consequently, designing the compensators for the decoupled control loops is simplified and can be made by single-input single-output control design procedures. Frequency-domain bode plot analysis is applied to design the system compensators. System compensators should provide desired steady-state error and sufficient phase margin, high stability, and high bandwidth.

In this system, compensators should have an integration unit to increase the system type in order to eliminate the steady-state error of the system step responses. Besides, in order to reach desired phase margin $60^\circ \le P.M \le 80^\circ$ and proper gain margin $G.M \ge 10$ db and enough cutoff frequency, the compensator construction should include a lead unit in addition to the integral unit. So, the general form of $(K(1+Ts)/s(1+aTs))$ is introduced for the all system compensators. Regarding the mentioned considerations about control compensator design, all the system compensators for three operation modes are demonstrated in Table I. The open-loop bode plot prior and pro to compensation has been plotted for the three operation modes in Figs. 8–10.

Investigating the obtained bode plots, it can be understood that integral units in the system compensators lead to achieve about -20 db/dec slope in low frequencies. Although it eliminates the steady-state error of the system step response, it causes a lower cutoff frequency for the system and decreases the

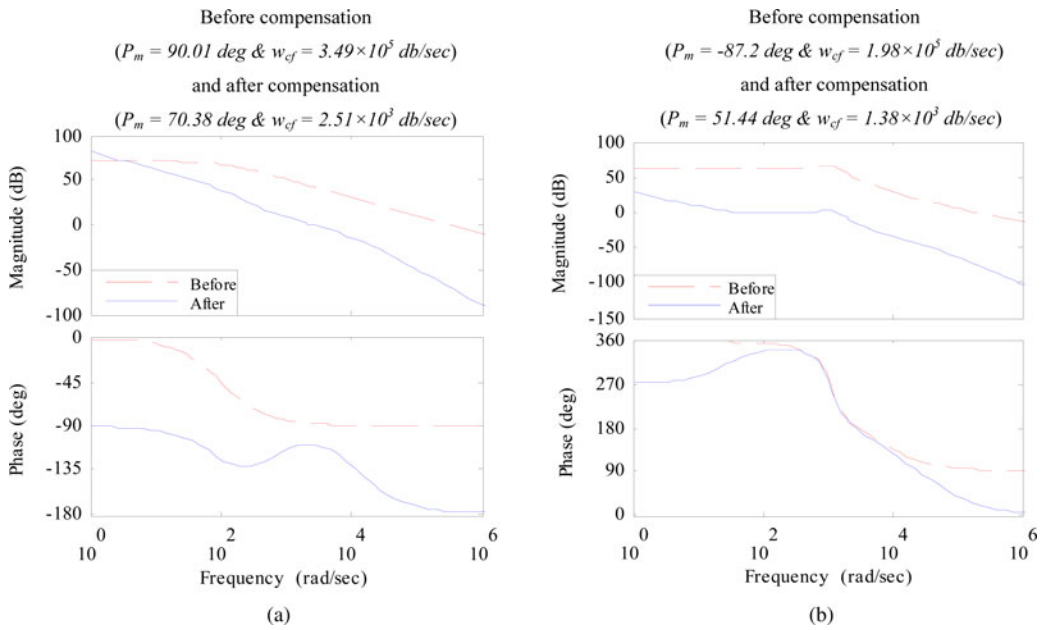

Fig. 8. Bode plots of the first operation mode. (a) $i_{L1}(s)/d_1(s)$ and (b) $v_o(s)/d_2(s)$.

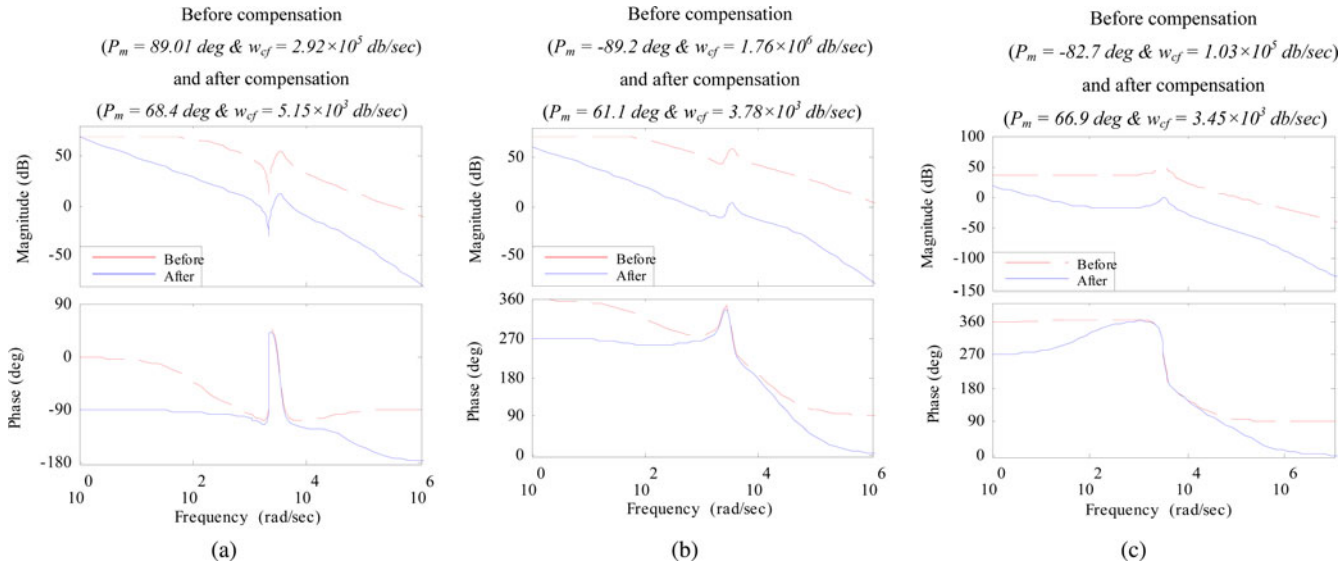

Fig. 9. Bode plots of the first operation mode. (a) $i_{L1}(s)/d_1(s)$, (b) $i_{L2}(s)/d_2(s)$, and (c) $v_o(s)/d_4(s)$.

system phase margin. The bandwidth limitation (lower cutoff frequency) causes to decrease the speed of the system responses and low phase margin leads the system to unstability. Therefore, utilizing lead-type compensator results in increasing the cutoff frequency and phase margin. These parameters before and after compensation are shown in the figures. Although the cutoff frequency before the compensation is higher than after compensation, the control-loop bandwidth limitation is helpful to reduce the loop interactions. On the other hand, as clear from the figures, low gain of the system in high frequencies increases the robustness of the system and decreases the influence of noise. Finally, utilizing the compensators result in achieving phase margin up to 60°, gain margin up to 10 db, and reasonable cutoff frequency for the open-loop transfer functions of the system.

As mentioned, the proposed converter is mainly recommended to be utilized in PV/FC/battery hybrid power systems. It is obviously clear that the converter control design should be done regarding some specific conditions and restrictions related to the PV, the FC, and the battery sources. Next section has been organized to discuss about these conditions and restrictions such as MPPT of the PV source, maximum deliverable powers of the FC and the battery, and the load condition. Therefore, all the converter controllers have been designed for the present hybrid power system in the next section. For such a hybrid PV/FC/battery power system, the amount of the PV power

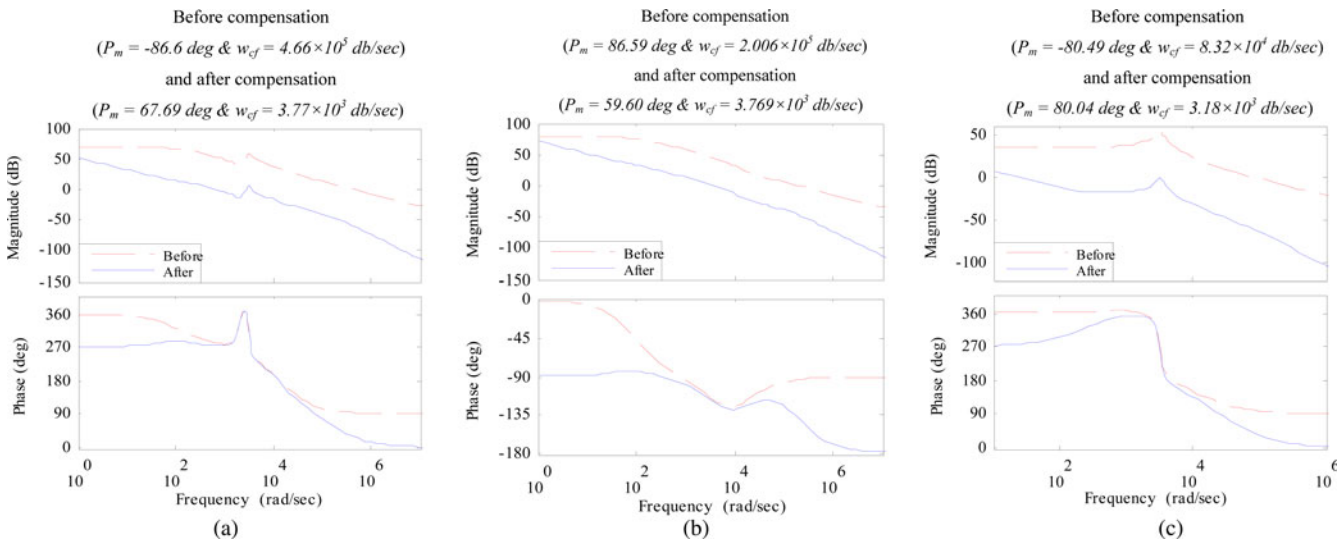

Fig. 10. Bode plots of the first operation mode. (a) $i_{L1}(s)/d_1(s)$, (b) $i_{L2}(s)/d_2(s)$, and (c) $v_o(s)/d_3(s)$.

generation and the load power is not constant and can be changed with an unknown pattern. Therefore, the operating point of the converter is changeable which may result in changing the converter small-signal model. For this reason, the validity of the designed control system of the converter should be certified for the all possible operating points. As a verification method, the robust analysis of the converter control system can be done for wide range variations of the converter operating point which its results are absolutely valid for narrow changes in the converter operating point as like as what is done in the sensitivity analysis.

In general, robust stability analysis for the various dc–dc converters can be done using Kharitonov's theorem [33]. However, another useful method to analysis the robust stability for systems with order $n \leq 5$ is Hermite–Biehler theorem which has been utilized for analyzing the robust stability of the push–pull dc–dc converter [34]. This method is applicable to the all dc–dc converters which have the transfer function with the order $n \leq 5$. This method also gives three useful stability margin criteria in addition to ensure the system stability. For the proposed converter, the closed-loop converter can be approximated with a system with order $n = 5$ (five dominant poles can be found), which makes this method applicable to ensure the converter control stability. This analysis has been performed for the all three operation modes of the proposed converter. However, based on the achieved results, this can be deduced that the designed converter closed-loop control system is highly stable for the all possible operating points.

V. System Power Operation Mode Determination

In this section as the converter application, it has been utilized to interface a PV source at the first input port, an FC source at the second input port, and a lead–acid battery at the storage port. In this system, the PV and the FC sources are responsible for supplying a residential load and the battery is employed to supply a part of power demand in the PV poor generation and high-load circumstances in addition to improving startup transitions and dynamic characteristic of the FC. Such a hybrid system necessitates an overall control system to provide MPPT for the PV source [35], regulate the output voltage, set the FC in its reference power [36], and consider the state of charge (SOC) regulation of the battery [37], [38]. These goals of operation will be optimally realized if the proper operation mode is chosen for the converter. Therefore, the proper operation mode should be determined regarding to the maximum available PV power, the maximum deliverable FC power ($P_{FC}^{\max}$), the output voltage value, and the battery charging necessity. In this system, an SOC regulation for the battery is considered to keep the battery voltage in allowable minimum and maximum voltages $v_{\mathrm{Batt.Min}} < v_{\mathrm{Batt}} < v_{\mathrm{Batt.Max}}$ [37]. Through this strategy, if the battery voltage is less than $v_{\mathrm{Batt.Min}}$, the state of battery charging is required. In this condition, if the summation of the PV and the FC powers can manage to supply and charge the load and battery, respectively, at the same time, the battery charging is started. The amount of the battery charging power depends on the battery capacity C_B, which is usually chosen less than $0.2C_BV_B$ (refer to lead–acid battery handbooks). Besides, the battery discharge state depends on the PV and FC power generation and load and it can be started when the battery voltage is higher than $v_{\mathrm{Batt.Min}}$. Suggested algorithm for determining proper operation mode is explained as follows.

First operation mode: This mode is defined as the basic operation mode and takes place in the conditions that the summation of the PV and the FC powers can completely supply the load, and charging the battery is not necessary. The goals of this operation mode are extracting the maximum power of the PV source and regulating the output voltage by the FC power. Therefore, the current of the PV source is controlled by duty ratio d_1 to achieve MPPT and duty ratio d_2 is utilized for regulating the output voltage.

Second operation mode: This operation mode takes place in the conditions that the output voltage cannot be regulated because summation of the FC and the PV maximum achievable powers cannot completely supply the load. In this condition, maximum deliverable powers of the FC and the PV should be

extracted by controlling duty ratios d_1 and d_2, and the battery should be discharged to regulate the output voltage by duty ratio d_4. This performance will be only accomplished if the battery voltage is more than $v_{\mathrm{Batt.Min}}$, unless the system should be shouted down.

Third operation mode: This operation mode takes place in the conditions that the summation of the FC and the PV powers can regulate the output voltage as like as first operation mode, while the battery is needed to be charged. In this mode, the control strategy is based on achieving MPPT of the PV source by duty ratio d_1, setting the FC on its reference power by duty ratio d_2, and regulating the output voltage by duty ratio d_3 which simultaneously provides battery charging performance. In this mode, considering the fact that if the PV and the FC completely supply the load, the output voltage will be regulated and charging power of the battery will be set at zero. In this condition, adding an optional amount power to the FC reference power results in charging the battery with this additional power as the battery is employed to regulate the output voltage. This optional amount power depends on the battery capacity C_B, which is usually chosen less than $0.2C_BV_B$ (regarding to the battery SOC regulation).

In the conditions that the load power is less than the maximum available power of the PV, the system is programmed to regulate the output voltage and charge the battery (if required). Besides, in situation that the battery charging is not required, the PV power is utilized to regulate the output voltage. Therefore, only the first duty ratio d_1 is employed to regulate the output voltage with a simple voltage controller as like as in controlling of a single boost converter. Such operating conditions can result in the PV source operating out of its MPPT performance.

VI. Simulation and Experimental Verifications

A. Simulation Results

In order to verify the performance of the proposed converter, simulations have been done in all three operation modes by PSCAD/EMTDC software. A resistive domestic load R_L with the peak power of 3.5 kW and the average power of 2.3 kW is supplied at the dc link by the proposed system. The dc-link voltage of the converter is desired to be regulated on $v_o = 350$ V. In order to assure reliable electricity supply, the size of the PV and the FC sources are assumed as $P_{\mathrm{PV}}^{\max} = 2.5\,\mathrm{kW}$, $P_{\mathrm{FC}}^{\max} = 2.5\,\mathrm{kW}$, and the maximum discharge power of the battery is $P_{\mathrm{Batt}}^{\max} = +1\,\mathrm{kW}$ in this paper. In the simulation, the PV and the FC are modeled [39], [40]. The output *P–I* characteristics of these sources are shown in Figs. 11 and 12, respectively. In Fig. 11, three different output characteristics are depicted for the PV source with the maximum powers 0.45, 1.7, and 2.35 kW. These output characteristics are achieved for the PV source for the irradiation levels 250, 700, and 900 W/m^2, respectively. As it is clear from the figure, for each output characteristic there is only one operating point in which the maximum power of the PV source is extractable. Hence, PV source should be exploited in MPPT condition. In this operating condition, the slope of the output characteristics has zero value ($dP_{\mathrm{PV}}/dI_{\mathrm{PV}} = 0$). In this paper, the incremental conductance (IC) MPPT algorithm [41] has been used to track the maximum power of PV source. With this method, the reference current of PV source is adjusted in a way that the operating point of PV source is set at its maximum power point (MPP). Based on IC MPPT method, when the operating point of PV source is on the left hand of the MPP ($dP_{\mathrm{PV}}/dI_{\mathrm{PV}} > 0$), the reference current of the PV should be increased. On the other hand, when PV source works on an operating point on the right hand of the MPP ($dP_{\mathrm{PV}}/dI_{\mathrm{PV}} < 0$), the reference current should be decreased. In the condition that PV source operates at its MPP, there is need to have change in the reference current. Determination of the operating point position of PV source regarding to the MPP can be accomplished by a periodic control process. Also, Fig. 12 shows the output *P–I* characteristic of the FC source with the maximum extractable current $I_{\mathrm{FCmax}} = 33$ A. For the proposed system, depending on the PV and the load conditions, all the operating points on this output characteristic may be provided for the FC source to operate. Moreover, the battery voltage is $v_B = 48$ V, which its capacity can be chosen according to the time duration of its utilization. The simulation parameters of the converter are listed in Table II.

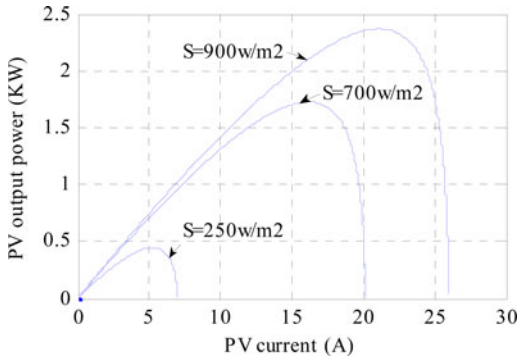

Fig. 11. PV *P–I* characteristic.

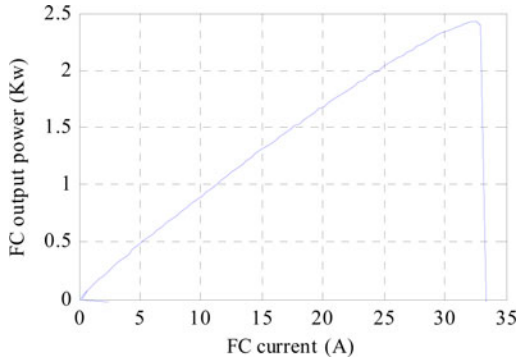

Fig. 12. FC *P–I* characteristic.

A 6-s simulation with three different stages is provided to evaluate the converter performance in each operation mode. Simulation results for the powers of input sources are shown in Fig. 13. Fig. 14 depicts the dc-link voltage which is effectively regulated on its reference value in the all simulation stages. Moreover, duty ratios d_1 and d_2, which regulate the PV and the FC powers, are illustrated in Fig. 15. In Fig. 16, duty ratios

TABLE II
SIMULATION AND SYSTEM PROTOTYPE PARAMETERS

Symbols	Simulation parameters	Prototype parameters
r_1	0.1Ω	0.2Ω
L_1	4mH	4mH
r_2	0.1Ω	0.2Ω
L_2	4mH	4mH
C	200μF	500μF
f_s	20kHz	20kHz

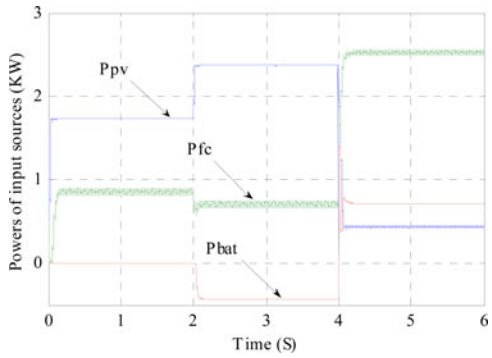

Fig. 13. Powers of input sources.

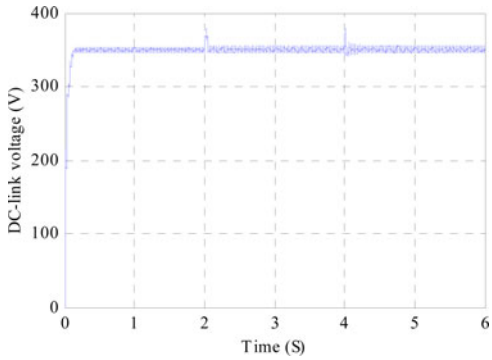

Fig. 14. DC-link voltage.

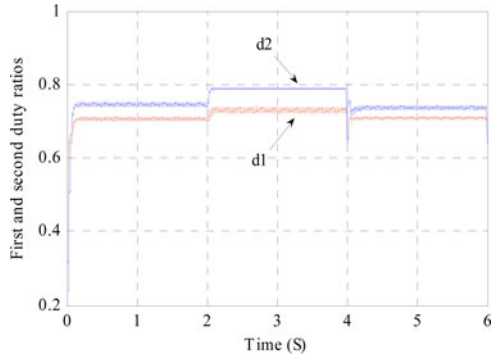

Fig. 15. First and second duty ratios.

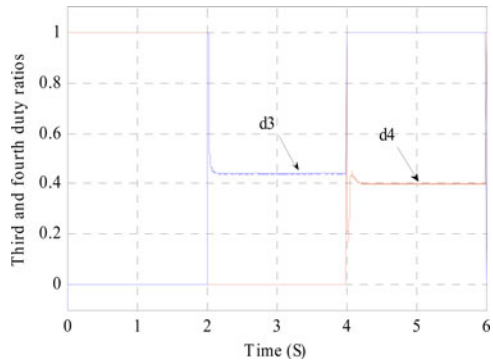

Fig. 16. Third and fourth duty ratios.

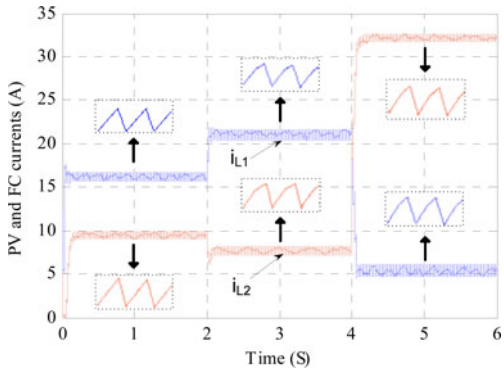

Fig. 17. PV and FC currents.

d_3 and d_4, regulating battery power, are exhibited. The PV and the FC currents and the current of the battery are illustrated in Figs. 17 and 18, respectively. According to the simulation results, these stages of the simulation are described in detail as follows.

First simulation stage $0 \leq t < 2$ s: In this stage, as shown in Fig. 13, the load power is $P_L = 2.5$ kW ($R_L = 49\ \Omega$), while the maximum available PV power is $P_{\rm PV} = 1.7$ kW ($S = 700$ W/m^2) and there is no need to charge the battery. Considering the FC maximum deliverable power, the power deficiency between the PV and load ($P_L - P_{\rm PV}$) can be supplied by the FC; so, the first operation mode is chosen for the converter. In addition to the power deficiency 0.8 kW, the FC should supply the power losses of the converter in order to regulate the output voltage. In this mode, according to the control system and as shown in Figs. 15 and 17, the FC current is set on $i_{L2} = 9.4$ A by duty ratio $d_2 = 0.75$ to regulate the output voltage, while the maximum power of the PV is elicited with the current of $i_{L1} = 16.25$ A and adjusting the first duty ratio at $d_1 = 0.7$. In addition, the third and fourth duty ratios, as shown in Fig. 16, are set on $d_3 = 0$ and $d_4 = 1$, which result the battery power to be set on zero value, as shown in Fig. 18.

Second simulation stage $2 \leq t < 4$ s: In this stage, as shown in Fig. 13, a step change in the sun irradiation level at $t = 2$ s results to increase the available maximum PV power into $P_{\rm PV} = 2.35$ kW ($S = 900$ W/m^2), while the load power remains constant at $P_L = 2.5$ kW. In addition, in this stage, the battery charging is assumed to be performed, so the third operation mode is chosen for the converter. In this condition, providing charging power

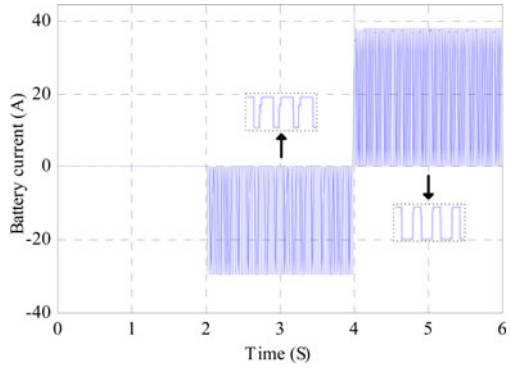

Fig. 18. Battery current.

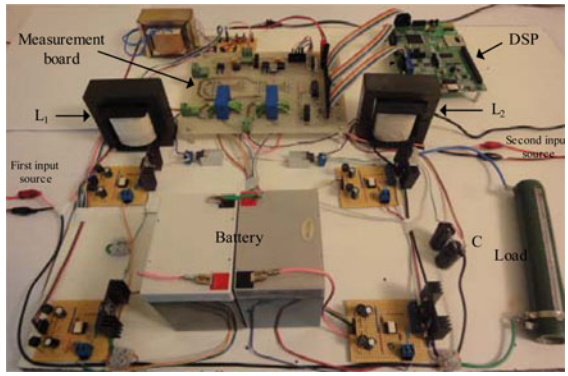

Fig. 19. Prototype system photograph.

of the battery about 0.35 kW in addition to power deficiency between the PV and the load (0.15 kW) and the converter power losses estimation about 0.2 kW results in defining the reference power of the FC at $P_{\rm FC}^{\rm ref} = 0.7\,{\rm kW}$. As shown in Fig. 13, the battery has been charged with the power of 0.42 kW. The extra charging power of the battery is resulted from the fact that the converter power losses is not exactly estimated, so the battery is charged with a higher power level in order to regulate the output voltage. According to the control system and Figs. 15 and 17, the FC current is regulated on $i_{L2} = 7.5\,{\rm A}$ with duty ratio $d_2 = 0.79$, while the maximum power of the PV source is tracked with regulating the PV current at $i_{L1} = 21\,{\rm A}$ and adjusting the first duty ratio at $d_1 = 0.73$. Moreover, as shown in Fig. 16, controlling the third and fourth duty ratios at $d_3 = 0.45$ and $d_4 = 0$, respectively, results in providing the charging power of the battery in addition to regulating the output voltage.

Third simulation stage $4 \leq t < 6$ s: This stage occurs in a condition that the load power is increased to the maximum value $P_L = 3.5\,{\rm kW}$ and the PV power is simultaneously decreased into $P_{\rm PV} = 0.45\,{\rm kW}$ ($S = 250\,{\rm W/m^2}$) at the time $t = 4$ s, as shown in Fig. 13. From the maximum deliverable power of the FC, it is obviously understood that the FC is not able to completely supply the power deficiency (3.05 kW); thus, the remained power should be supplied by the battery. Therefore, the second operation mode is chosen for the converter with $P_{\rm FC}^{\rm ref} = 2.5\,{\rm kW}$. In this mode, according to the corresponding control system and as shown in Figs. 15 and 17, MPPT of the PV is accomplished by regulating its current at $i_{L1} = 5.3\,{\rm A}$ and adjusting the first duty ratio at $d_1 = 0.71$, while the maximum power of the FC is delivered at $i_{L2} = 32\,{\rm A}$ with adjusting the second duty ratio at $d_2 = 0.73$. As shown in Fig. 16, controlling the third and fourth duty ratios at $d_3 = 1$ and $d_4 = 0.4$ results in discharging the battery with $P_{\rm Batt} = 0.73\,{\rm kW}$ in order to regulate the output voltage and supply the converter power losses.

As it is clear from Fig. 18, the battery current is discontinuous between zero and summation of the PV and the FC currents with the converter switching frequency in the second and third operation modes. A low-cost high-frequency low-pass filter can be used to effectively smooth the battery current. The cutoff frequency of such filter can be tuned two or three times bigger than the switching frequency.

Based on simulation results, the designed converter closed-loop control system is highly stable for the all possible operating points.

B. Experimental Results

In order to verify the effectiveness of the proposed converter, a low power range laboratory prototype was built as shown in Fig. 19. Two different input power sources with the maximum voltages of 40 V and maximum currents of 5 A are utilized instead of the PV and the FC sources. A 24-V battery consisting of two series 12-V lead–acid battery is employed in the prototype as the storage system. The control scheme is implemented by the Texas Instrument TMS320F2812 DSP. The parameters of the prototype are listed in Table II.

For the experimental setup, the input power sources are set at constant voltage values 40 and 35 V as the PV and the FC sources, respectively. The reference value of the output voltage is 120 V and a resistive load with the power of 220 W is used in the prototype. In order to validate the converter performance, three different operation modes of the converter are tested by changing the reference currents of the input power sources. The experimental setup is examined in three different subsequent stages relevant to the first, third, and second operation modes, respectively.

The experimental results for the currents of the first and second power sources, the current of the battery and the dc-link voltage are shown in Figs. 20–23, respectively. Further, the current ripples in each operation mode are illustrated in the aforementioned figures. All the experimental figures represented in following are shown with the scale of 0.1. The stages of the experimental results are described in detail as follows.

First stage: In this stage, for realizing the first operation mode, the reference current of the first power source is defined $i_{L1} = 3.5\,{\rm A}$; therefore, the control system regulates the output voltage around 120 V by drawing $i_{L2} = 3\,{\rm A}$ from the second power source. So, the power of $P_2 = 105\,{\rm W}$ is achieved from the second power source which supplies the power deficiency and the converter power losses.

Second stage: In this stage, the battery requires to be charged with the power around $P_{\rm Batt} = -50\,{\rm W}$. Therefore, for realizing the third operation mode, the current of the first power source is

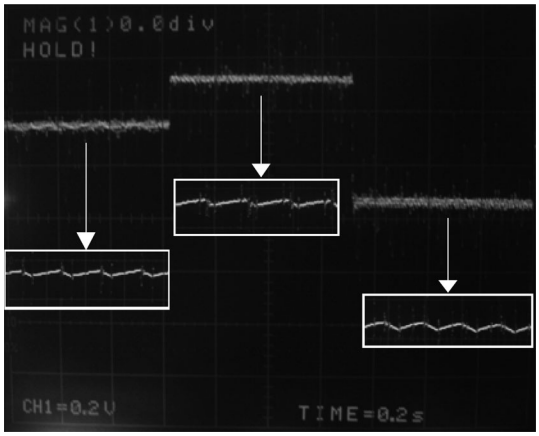

Fig. 20. Current of the first power source.

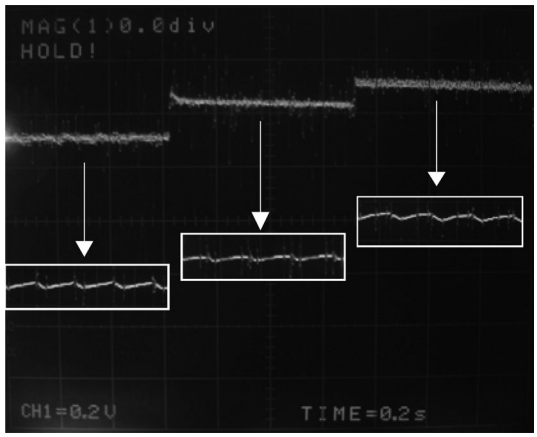

Fig. 21. Current of the second power source.

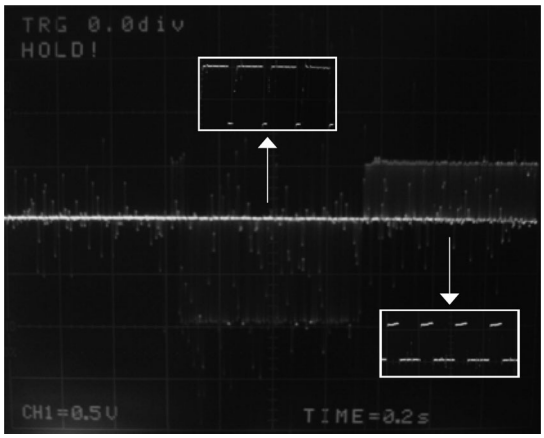

Fig. 22. Current of the battery.

changed to $i_{L1} = 5$ A which achieves $P_1 = 200$ W. Because the power of the first power source is not sufficient for supplying the load, charging the battery and compensating the converter losses, the second power source is employed. So, the current of the second power source is set at $i_{L2} = 4.2$ A.

Third stage: In this stage, for realizing the second operation mode, the power of the first power source is changed to $P_1 =$ 24 W with the current $i_{L1} = 0.6$ A. As extracting the maximum current of $i_{L2} = 5$ A from the second power source cannot supply the power deficiency, the battery should be discharged in this mode. Therefore, the battery is discharged with the power of $P_{\mathrm{Batt}} = 50$ W to regulate the output voltage.

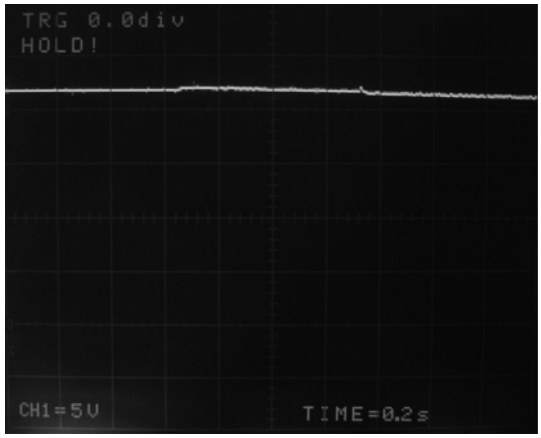

Fig. 23. Output voltage.

From the inductors currents in the second and third operation modes, two subsequent charging intervals can be clearly seen in the figures. The efficiency of the proposed converter in all three operation modes is up to 80%. The converter efficiency can be improved because it mainly depends on the laboratory power devices.

VII. Conclusion

A new three-input dc–dc boost converter with unified structure for hybrid power systems is proposed in this paper. The proposed converter is applied to hybridize a PV, an FC, and a battery storage system. Four independent duty ratios of the converter facilitate power flow among input sources and the load. Three different power operation modes are defined for the converter and its corresponding transfer function matrix is obtained in each operation mode. Two types of decoupling networks are utilized to separately design the converter closed-loop compensators. Utilizing these decoupling networks and frequency-domain bode plot analysis, the converter controllers are separately designed which lead to achieve phase margin $60^\circ \leq P.M \leq 80^\circ$ and gain margin $G.M \geq 10$ db and enough cutoff frequency for the system. As the simulation results show, the converter control system provides good transient and steady-state responses for the converter with respect to the different step changes in the PV power generation and the load condition. In addition, the designed converter closed-loop control system is highly stable for the all possible operating points. The simulation results are verified by a low power range laboratory prototype with an acceptable efficiency. The proposed converter has the merits of making use of low-voltage batteries, working in stable margin operating points in addition to the advantages of bidirectional power flow at the storage port, simple structure, and low-power components.

REFERENCES

[1] W. Jiang and B. Fahimi, "Active current sharing and source management in fuel cell-battery hybrid power system," *IEEE Trans. Ind. Electron.*, vol. 57, no. 2, pp. 752–761, Feb. 2010.

[2] R. J. Wai, Ch. Y. Lin, J. J. Liaw, and Y. R. Chang, "Newly designed ZVS multi-input converter," *IEEE Trans. Ind. Electron.*, vol. 58, no. 2, pp. 555–566, Feb. 2011.

[3] J. L. Duarte, M. Hendrix, and M. G. Simoes, "Three-port bidirectional converter for hybrid fuel cell systems," *IEEE Trans. Power Electron.*, vol. 22, no. 2, pp. 480–487, Mar. 2007.

[4] N. Kato, K. Kurozumi, N. Susuld, and S. Muroyama, "Hybrid power-supply system composed of photovoltaic and fuel-cell systems," in *Proc. Int. Telecommun. Energy Conf.*, 2001, pp. 631–635.

[5] K. Rajashekara, "Hybrid fuel-cell strategies for clean power generation," *IEEE Trans. Ind. Appl.*, vol. 41, no. 3, pp. 682–689, May/Jun. 2005.

[6] P. Thounthong, S. Rael, and B. Davat, "Control strategy of fuel cell and supercapacitor association for a distributed generation system," *IEEE Trans. Ind. Electron.*, vol. 56, no. 6, pp. 3225–3233, Dec. 2007.

[7] O. C. Onara, M. Uzunoglu, and M. S. Alam, "Modeling, control and simulation of an autonomous wind turbine/photovoltaic/fuel cell/ultra capacitor hybrid power system," *J. Power Sources.*, vol. 185, no. 2, pp. 1273–1283, Apr. 2008.

[8] K. N. Reddy and V. Agrawal, "Utility-interactive hybrid distributed generation scheme with compensation feature," *IEEE Trans. Energy Convers.*, vol. 22, no. 3, pp. 666–673, Sep. 2007.

[9] R. Gopinath, S. Kim, J. H. Hahn, P. N. Enjeti, M. B. Yeary, and J. W. Howze, "Development of a low cost fuel cell inverter system with DSP control," *IEEE Trans. Power Electron.*, vol. 19, no. 5, pp. 1256–1262, Sep. 2004.

[10] X. Huang, X. Wang, T. Nergaard, J. S. Lai, X. Xu, and L. Zhu, "Parasitic ringing and design issues of digitally controlled high power interleaved boost converters," *IEEE Trans. Power Electron.*, vol. 19, no. 5, pp. 1341–1352, Sep. 2004.

[11] F. Z. Peng, H. Li, G. J. Su, and J. S. Lawler, "A new ZVS bidirectional dc–dc converter for fuel cell and battery application," *IEEE Trans. Power Electron.*, vol. 19, no. 1, pp. 54–65, Jan. 2004.

[12] Y. C. Chuang and Y. L. Ke, "High-efficiency and low-stress ZVT-PWM DC-to-DC converter for battery charger," *IEEE Trans. Ind. Electron.*, vol. 55, no. 8, pp. 3030–3037, Aug. 2008.

[13] Y. Ch. Liu and Y. M. Chen, "A systematic approach to synthesizing multi-input DC–DC converters," *IEEE Trans. Power Electron.*, vol. 24, no. 1, pp. 116–127, Jan. 2009.

[14] Y. M. Chen, Y. Ch. Liu, S. C. Hung, and C. S. Cheng, "Multi-input inverter for grid-connected hybrid PV/Wind power system," *IEEE Trans. Power Electron.*, vol. 22, no. 3, pp. 1070–1077, May 2007.

[15] L. Yan, R. Xinbo, Y. Dongsheng, L. Fuxin, and C. K. Tse, "Synthesis of multiple-input DC/DC converters," *IEEE Trans. Power Electron.*, vol. 25, no. 9, pp. 2372–2385, Sep. 2010.

[16] A. Kwasinski, "Identification of feasible topologies for multiple-input DC–DC converters," *IEEE Trans. Power Electron.*, vol. 24, no. 3, pp. 856–861, Mar. 2010.

[17] Y. M. Chen, Y. Ch. Liu, and F. Y. Wu, "Multi-input DC/DC converter based on the multiwinding transformer for renewable energy applications," *IEEE Trans. Ind. Electron.*, vol. 38, no. 4, pp. 1096–1103, Jul./Aug. 2002.

[18] H. Matsuo, W. Lin, F. Kurokawa, T. Shigemizu, and N. Watanabe, "Characteristics of the multiple-input DC–DC converter," *IEEE Trans. Ind. Electron.*, vol. 51, no. 3, pp. 625–631, Jun. 2004.

[19] H. Krishnaswami and N. Mohan, "Three-port series-resonant DC–DC converter to interface renewable energy sources with bidirectional load and energy storage ports," *IEEE Trans. Power Electron.*, vol. 24, no. 10, pp. 2289–2297, Mar. 2009.

[20] H. Tao, A. Kotsopoulos, J. L. Duarte, and M. A. M. Hendrix, "Family of multiport bidirectional DC–DC converters," in *Proc. IEE Elect. Power Appl.*, 2006, pp. 451–458.

[21] M. Sarhangzadeh, S. H. Hosseini, M. B. B. Sharifian, and G. B. Gharehpetian, "Multi-input direct DC–AC converter with high frequency link for clean power generation systems," *IEEE Trans. Power Electron.*, vol. 26, no. 6, pp. 1777–1789, Jun. 2011.

[22] L. Solero, A. Lidozzi, and J. A. Pomilio, "Design of multiple-input power converter for hybrid vehicles," *IEEE Trans. Power Electron.*, vol. 20, no. 5, pp. 1007–1016, Sep. 2005.

[23] A. Khaligh, J. Cao, and Y. J. Lee, "A multiple-input DC–DC converter topology," *IEEE Trans. Power Electron.*, vol. 24, no. 3, pp. 862–868, Mar. 2009.

[24] S. H. Hosseini, S. Danyali, F. Nejabatkhah, and S. A. K. Mozafari Niapour, "Multi-input DC boost converter for grid connected hybrid PV/FC/battery power system," in *Proc. IEEE Elect. Power Energy Conf.*, 2010, pp. 1–6.

[25] H. Tao, J. L. Duarte, and M. A. M. Hendrix, "Three-port triple-half-bridge bidirectional converter with zero-voltage switching," *IEEE Trans. Power Electron.*, vol. 23, no. 2, pp. 782–792, Mar. 2008.

[26] R. J. Wai, Ch. Y. Lin, and Y. R. Chang, "High step-up bidirectional isolated converter with two input power sources," *IEEE Trans. Ind. Electron.*, vol. 56, no. 7, pp. 2629–2643, Jul. 2009.

[27] Zh. Qian, O. A. Rahman, H. A. Atrash, and I. Batarseh, "Modeling and control of three-port DC/DC converter interface for satellite applications," *IEEE Trans. Power Electron.*, vol. 25, no. 3, pp. 637–649, Mar. 2010.

[28] Zh. Qian, O. A. Rahman, and I. Batarseh, "An integrated four-port DC/DC converter for renewable energy applications," *IEEE Trans. Power Electron.*, vol. 25, no. 7, pp. 1877–1887, Jul. 2010.

[29] N. Mohan, T. M. Undeland, and W. P. Robbins, *Power Electronics: Converters, Applications, and Design*. New York: Wiley, 1995.

[30] A. Di Napoli, F. Crescimbini, F. G. Capponi, and L. Solero, "Control strategy for multiple input dc–dc power converters devoted to hybrid vehicle propulsion system," in *Proc. IEEE Int. Symp. Ind. Electron.*, L'Aquila, Italy, 2002, pp. 1036–1041.

[31] M. H. Rashid, Ed., *Power Electronics Handbook*. San Diego, CA: Academic, 2001.

[32] K. Warwick and D. Rees, *Industrial Digital Control Systems* (IEE Control Engineering Series 37). Stevenage, U.K: Peregrinus, 1988.

[33] V. L. Kharitonov, "Asymptotic stability of an equilibrium position of a family of systems of linear differential equations," *Differ. Equa.*, vol. 4, pp. 2086–2088, 1978.

[34] Y. V. Hote, D. R. Choudhury, and J. Gupta, "Robust stability analysis of the PWM push-pull DC–DC Converter," *IEEE Trans. Power Electron.*, vol. 24, no. 10, pp. 2353–2356, Oct. 2009.

[35] C. Wang, "Modeling and control of hybrid wind/photovoltaic/fuel cell distributed generation systems," Ph.D. dissertation, Montana State Univ., Bozeman, 2006.

[36] L. N. Khanh, J. J. Seo, Y. S. Kim, and D. J. Won, "Power-management strategies for a grid-connected PV-FC hybrid system," *IEEE Trans. Ind. Electron.*, vol. 25, no. 3, pp. 1874–1882, Jul. 2010.

[37] K. Jin, X. Ruan, M. Yang, and M. Xu, "A hybrid fuel cell power system," *IEEE Trans. Power Del.*, vol. 56, no. 4, pp. 1212–1222, Apr. 2009.

[38] M. Durr, A. Cruden, S. Gair, and J. R. McDonald, "Dynamic model of a lead acid battery for use in a domestic fuel cell system," *Elsevier J. Power Sources*, vol. 161, no. 2, pp. 1400–1411, Oct. 2006.

[39] M. A. S. Masoum, H. Dehbonei, and E. F. Fuchs, "Theoretical and experimental analyses of photovoltaic systems with voltage and current-based maximum power-point tracking," *IEEE Trans. Energy Convers.*, vol. 17, no. 4, pp. 514–522, Dec. 2002.

[40] J. Jia, Q. Li, Y. Wang, Y. T. Cham, and M. Han, "Modeling and dynamic characteristic simulation of a proton exchange membrane fuel cell," *IEEE Trans. Energy Convers.*, vol. 24, no. 1, pp. 283–291, Mar. 2009.

[41] Y. C. Kuo and T. J. Liang, "Novel maximum-power-point-tracking controller for photovoltaic energy conversion system," *IEEE Trans. Ind. Electron.*, vol. 48, no. 3, pp. 594–601, Jul. 2001.

Farzam Nejabatkhah (S'09–M'10) was born in Tabriz, Iran, in 1987. He received the B.Sc. and M.Sc. degrees (first-class Hons.) in electrical power engineering from the University of Tabriz, Tabriz, Iran, in 2009 and 2011, respectively.

He is a member of Organization Exceptional Talents at the University of Tabriz. His main research interests include renewable energies and distributed generation, power electronic converters, and power management. He currently focuses on the multi-input converters.

Saeed Danyali was born in Abdanan, Ilam, Iran, in 1983. He received the B.Sc. degree in electronic engineering from the University of Yazd, Yazd, Iran, in 2005, and the M.Sc. degree in electrical power engineering from the University of Tabriz, Tabriz, Iran, in 2008. He is currently working toward the Ph.D. degree in electrical power engineering at the Faculty of Electrical and Computer Engineering, University of Tabriz, Tabriz, Iran.

His research interests include the areas of renewable energy systems, power electronic converters, and brushless dc motor drives. He currently focuses on the single-stage multiinput converters.

Seyed Hossein Hosseini (M'93) was born in Marand, Iran, in 1953. He received the M.S. degree from the Faculty of Engineering, University of Tabriz, Tabriz, Iran, in 1976, and the D.E.A. and Ph.D. degrees from Institut National Polytechnique de Lorraine, Nancy, France, in 1978 and 1981, respectively, all in electrical engineering.

In 1982, he joined the Department of Electrical Engineering, University of Tabriz, as an Assistant Professor, where he was an Associate Professor from 1990 to 1995, and has been a Professor since 1995. From September 1990 to September 1991 he was a Visiting Professor at the University of Queensland, Brisbane, Australia. From September 1996 to September 1997, he was a Visiting Professor at the University of Western Ontario, London, ON, Canada. His research interests include power electronic converters, matrix converters, active and hybrid filters, application of power electronics in renewable energy systems and electrified railway systems, reactive power control, harmonics, and power quality compensation systems such as static var compensator, unified power quality conditioner, and flexible AC transmission systems devices.

Mehran Sabahi was born in Tabriz, Iran, in 1968. He received the B.Sc. degree in electronic engineering from the University of Tabriz, Tabriz, Iran, the M.Sc. degree in electrical engineering from Tehran University, Tehran, Iran, and the Ph.D. degree in electrical engineering from the University of Tabriz, in 1991, 1994, and 2009, respectively.

In 2009, he joined the Faculty of Electrical and Computer Engineering, University of Tabriz, where he has been an Assistant Professor since 2009. His current research interests include power electronic converters and renewable energy systems.

Seyedabdolkhalegh Mozaffari Niapour (S'09–M'10) was born in Shiraz, Iran, on July 23, 1984. He received the B.Sc. degree (Hons.) from the Islamic Azad University, Kazerun, Iran, in 2007, and the M.Sc. degree (first-class Hons.) from the University of Tabriz, Tabriz, Iran, in 2011, both in electrical power engineering.

He is a member of Organization Exceptional Talents at the University of Tabriz. His main research interests include brushless dc motors and generators, electric and hybrid vehicles, renewable energy systems, and power electronic converters. He currently focuses on the sensorless control of high-performance brushless dc motor drives.